ELSEVIER

Contents lists available at ScienceDirect

# Archives of Biochemistry and Biophysics

journal homepage: www.elsevier.com/locate/yabbi



# Structural basis of double-stranded RNA recognition by the RIG-I like receptor MDA5

Xiaojun Li<sup>a</sup>, Cheng Lu<sup>a,1</sup>, Mikaela Stewart<sup>a,1</sup>, Hengyu Xu<sup>b</sup>, Roland K. Strong<sup>b</sup>, Tatyana Igumenova<sup>a</sup>, Pingwei Li<sup>a,\*</sup>

### ARTICLE INFO

Article history: Received 30 April 2009 and in revised form 9 June 2009 Available online 14 June 2009

Keywords: Innate immunity Nucleic acid receptor MDA5 CTD Crystal structure

#### ABSTRACT

RIG-I, MDA5 and LGP2 are cytosolic pattern recognition receptors detecting single-stranded or double-stranded RNA in virally infected cells. The activation of RIG-I or MDA5 stimulates the secretion of type I interferons that play key roles in antiviral immune responses. The C-terminal domains (CTD) of RIG-I and LGP2 are responsible for RNA binding; however, it is not clear how MDA5 binds RNA. To understand the structural basis of dsRNA recognition by MDA5, we have determined the 1.45 Å resolution structure of the C-terminal domain of human MDA5. The structure revealed a highly conserved fold similar to the structures of RIG-I and LGP2 CTDs. NMR titration of MDA5 CTD with dsRNA demonstrated that a positively charged surface is involved in dsRNA binding. Mutagenesis and RNA binding studies showed that electrostatic interactions play primary roles in dsRNA recognition by MDA5. Like RIG-I and LGP2, MDA5 CTD preferentially binds dsRNA with blunt ends, but does not associate with dsRNA with either 5' or 3' overhangs. Molecular modeling of MDA5 CTD/dsRNA complex suggests that MDA5 CTD may recognize the first turn of blunt-ended dsRNA in a similar manner as LGP2.

Published by Elsevier Inc.

## Introduction

The innate immune system responds to a wide range of microbial infections and provides the first line of defense against infections by stimulating the induction of various cytokines and chemokines [1,2]. Type I interferons (IFNs), such as IFN- $\alpha$  and IFN-β, play critical roles in antiviral immune responses by inducing apoptosis of the infected cells, stimulating resistance to viral infection on surrounding cells, and activating acquired immune responses [3-5]. Viral nucleic acids, including double-stranded RNA and single-stranded RNA are potent inducers of IFNs. Two distinct families of pattern recognition receptors, the Toll-like receptors (TLRs) and the RIG-I like receptors (RLRs), are responsible for detecting viral nucleic acids in innate immunity [6-9]. Unlike TLRs that detect viral RNA in the endosome of specific cell types such as dendetric cells and macrophages, the RLRs are expressed ubiquitously and sense viral RNA in the cytoplasm of most cells types [10-12].

The RIG-I family receptors consist of three proteins, RIG-I, MDA5, and LGP2, of the DExD/H box RNA helicase family [10,11]. Both RIG-I and MDA5 encode tandem caspase recruitment do-

mains (CARD) on their N-termini followed by a DExD/H box RNA helicase domain and a C-terminal regulatory domain (CTD)<sup>2</sup>. The CTDs of RLRs play primary roles in RNA recognition while the CARDs are needed for signal transduction [9,13]. In contrast to MDA5 and RIG-I, LGP2 lacks the CARD domains and thus exhibits no signaling capability; however, it can negatively regulate the signaling of RIG-I or enhance the response to polyinosinic:polycytidylic acid (poly I:C) by MDA5 [14-16]. Studies of RIG-I and MDA5 knockout mice demonstrated these two proteins detect different but overlapping sets of viruses, suggesting they play different roles in antiviral immune responses [6,17,18]. RIG-I discriminates between viral and host RNA through recognition of single-stranded RNA with 5' triphosphate group, a signature of viral RNA [19-21]. In addition, chemically synthesized dsRNA and dsRNA derived from virus infected cells also activate RIG-I [9,17,22]. Synthetic dsRNA mimics such as polyinosinic-polycytidylic acid (poly I:C) or viral dsRNA of several kilobases in length activate MDA5 in cells [17,23]. In contrast, short poly I:C of a few hundred base pairs in length only activates RIG-I [23]. It is likely that MDA5 is responsible for the detection of long dsRNA while RIG-I is activated by short dsRNA in

<sup>&</sup>lt;sup>a</sup> Department of Biochemistry and Biophysics, Texas A&M University, College Station, TX 77843-2128, USA

<sup>&</sup>lt;sup>b</sup> Divison of Basic Sciences, Fred Hutchinson Cancer Research Center, Seattle, WA 98109, USA

<sup>\*</sup> Corresponding author. Fax: +1 979 845 9274. E-mail address: pingwei@neo.tamu.edu (P. Li).

<sup>&</sup>lt;sup>1</sup> These authors contributed equally to the work.

<sup>&</sup>lt;sup>2</sup> Abbreviations used: MDA5, Melanoma differentiation-associated protein 5; RIG-I, Retinoic acid-inducible gene 1; LGP2, Laboratory of genetics and physiology 2; CTD, C-terminal domain; NF-κB, nuclear factor kappa-light-chain-enhancer of activated B cells; TLR, Toll-like receptor; 5' ppp ssRNA, 5' triphosphorylated single-stranded RNA; dsRNA, double-stranded RNA. mAb, monoclonal antibody.

addition to 5' ppp ssRNA. The molecular mechanism of how viral RNA activates the RLRs is still largely unknown. It was suggested that under resting conditions RLRs are in a suppressed conformation and RNA binding induces a major conformational change of the RLRs, exposing their CARDs for the recruitment of the mitochondria bound adaptor protein IPS-1, which relays the signal to downstream proteins [11,13]. Stimulation of the RLRs ultimately leads to the activation of transcription factors IRF3, IRF7, and NF-κB that regulate the induction of type I interferons and proinflammatory cytokines [4,6,10].

The structure of RIG-I CTD has been determined by crystallography and NMR spectroscopy, providing insight into how RIG-I senses viral RNA [22,24]. Recently, the crystal structures of LGP2 CTD in isolation and in complex with an 8 bp dsRNA were also solved [16,25]. Strikingly, the LGP2 CTD/dsRNA complex structure revealed that LGP2 specifically recognizes the blunt ends of dsRNA. LGP2 CTD exhibits a high degree of charge and shape complementarity to the first turn of dsRNA and interacts with the backbone of the dsRNA through extensive electrostatic interactions and hydrogen bonding. The exposed bases at the terminus of the dsRNA interact with LGP2 primarily through hydrophobic interactions. Similar to LGP2, the RIG-I CTD also recognizes dsRNA with blunt ends in addition to 5' ppp ssRNA but does not bind dsRNA with either 5' or 3' overhangs efficiently. Moreover, NF-κB and IFN-β reporter assays showed that RIG-I was activated by short dsRNA with blunt ends but not by dsRNA with 3' or 5' overhangs. Although the structures of MDA5 and RIG-I bound to RNA are still not available, it is most likely that these two proteins might recognize the termini of dsRNA in a similar way as LGP2. To elucidate the structural basis of dsRNA recognition by MDA5, we have determined the high-resolution structure of MDA5 CTD by X-ray crystallography and mapped its binding surface for dsRNA by NMR spectroscopy. RNA binding studies and mutational analysis demonstrated that MDA5 recognizes the blunt end of dsRNA and a highly conserved positively charged surface is involved in dsRNA binding by MDA5 as well as RIG-I and LGP2. Molecular modeling of MDA5 CTD bound to dsRNA suggested that MDA5 might recognize the blunt end of dsRNA in a similar manner as its homolog LGP2.

# Materials and methods

Protein expression and purification

DNA encoding the C-terminal domain of human MDA5 (residues 892–1017) were cloned into expression vector pET22b(+) (Novagen). The C-terminal eight residues of MDA5 (residues 1018–1025) were excluded from the constructs to prevent protein dimerization via cysteine residues 1018 and 1019. The cloned DNA sequences were confirmed by plasmid DNA sequencing. MDA5 CTD was expressed in *Escherichia coli* strain BL21(DE3) by induction at OD $_{600}$  = 0.6–0.8 with 0.5 mM isopropyl- $\beta$ -D-thiogalactoside (IPTG) overnight at 15 °C. The protein was purified by Ni<sup>2+</sup> affinity chromatography followed by gel filtration chromatography. Mutants of MDA5 CTD were generated using Quickchange mutagenesis kit (Stratagene). Sequences of the mutants were confirmed by plasmid DNA sequencing. The mutant proteins were expressed and purified the same way as the native protein.

RNA binding studies by gel filtration chromatography

RNAs used in the binding studies were chemically synthesized by IDT (Coralville, IA) or by *in vitro* transcription using T7 RNA polymerase. The sequences of the RNAs are shown in Table 1. Double-stranded RNAs were generated by heating the ssRNA at 95 °C for 5 min and annealing at room temperature for 30 min. Each

**Table 1**Sequences of RNA used in binding studies by gel filtration chromatography, surface plasmon resonance and NMR spectroscopy.

8 bp dsRNA	5' GCGCGCGC 3'
	CGCGCGCG
8 nt ssRNA	5' ACACACAC 3'
	AAA
24 nucleotides small	5' CCGCAUUG A
hairpin RNA	3' GGCGTAAC G
	GUU
8 bp dsRNA with two	5' AAGCGCGCGC 3'
5' overhangs	CGCGCGCAA
8 bp dsRNA with two	5' GCGCGCGCAA 3'
3' overhangs	AACGCGCGCG
24 bp blunt-ended	5' GCGCGCAUGCGCGCAUGCGCGC 3'
dsRNA	CGCGCGUACGCGCGUACGCGCG
10 bp dsRNA	5' GGCGCGCGCC 3'
	CCGCGCGCGG

dsRNA was mixed with excess protein (RNA to protein molar ratio of 1–3) and 100  $\mu$ l of samples were injected over a Superdex200 (10/300 GL) column (GE healthcare) eluted with a buffer containing 50 mM Tris and 150 mM NaCl at pH 7.50. The column was calibrated with a set of protein standards for gel filtration chromatography (Bio-Rad).

RNA binding studies by surface plasmon resonance

The binding studies were conducted at 25 °C in HBS–EP<sup>+</sup> buffer (10 mM HEPES pH 7.4, 150 mM NaCl, 3 mM EDTA, 0.05% v/v P-20 surfactant) on a Biacore T100 system (Biacore AB). To determine the binding affinity of the 8 bp 5′ ppp ssRNA with MDA5 CTD, the goat anti-GST Ab (Biacore AB) at 30  $\mu g/mL$  in 10 mM sodium acetate (pH 5.0) was immobilized on a CM5 sensor chip by amine coupling. GST-tagged MDA5 CTD at 5  $\mu g/mL$  was captured over the immobilized anti-GST mAb at a flow rate of 10  $\mu L/min$  for 30 s to reach 1000 RU response. Serial dilutions of the 8 bp 5′ ppp dsRNA (0.31–80  $\mu M$ , including buffer as blank) were injected in randomized duplicate runs at a flow rate of 20  $\mu L/min$  for 5 min to reach equilibrium. Optimal regeneration was achieved by injection of 10 mM Glycine at pH 2.2 over the sensor chip.

To determine the binding affinities of the 24 bp dsRNA and the hairpin RNA with MDA5 CTD, an anti-His mAb (GenScript) at 100  $\mu g/mL$  in 10 mM sodium acetate (pH 4.0) was immobilized on a CM5 sensor chip by amine coupling. His-tagged MDA5 CTD at 5  $\mu g/mL$  was captured over the immobilized anti-His mAb at a flow rate of 30  $\mu L/min$  for 2 min to reach 500 RU response. Serial dilutions of the 24 bp dsRNA and the hairpin RNA analytes (0.125–4  $\mu M$  and 0.25–8  $\mu M$ , respectively), were injected in randomized duplicate runs at a flow rate of 50  $\mu L/min$  for 2 min to reach equilibrium. Optimal regeneration was achieved by injection of 0.085%  $H_3PO_4$  over the sensor chip.

Sensorgrams obtained from equilibrium SPR measurements were analyzed by the double-subtraction method described by Myszka [26]. The signal from the reference flow cell was subtracted from the analyte binding response. Data were then averaged for the two injections. Averaged data were then subtracted from the buffer blank signal and analyzed with BIAevaluation 3.0 software (Biacore). Steady state binding levels of analytes were plotted against analyte concentration, from which the equilibrium binding constant was estimated.

Crystallization, data collection, and structure determination

Purified MDA5 CTD was concentrated to  $\sim$ 30 mg ml<sup>-1</sup> in a buffer containing 20 mM Tris, 150 mM NaCl and 1 mM TCEP at pH 7.5.

The complex was crystallized in 0.1 M Tris buffer at pH 8.5 with 14-18% (v/v) ethanol by hanging drop vapor diffusion method at 4 °C. The crystals were flash-frozen in crystallization buffer supplemented with 25% (v/v) glycerol. MDA5 CTD crystallized in space group P2<sub>1</sub>, with cell dimensions: a = 28.41 Å, b = 60.92 Å, c = 36.44 Å and  $\beta = 102.58^{\circ}$ ; the crystallographic asymmetric unit contains one MDA5 CTD molecule. A complete data set to 1.45 Å resolution were collected using a Rigaku RAXIS IV++ image plate detector mounted on a Rigaku Micromax-007HF generator. The diffraction data were processed with the HKL package [27]. The structure of MDA5 CTD was determined by molecular replacement with MOLREP in the CCP4 suite [28] using RIG-I CTD as search model (PDB code: 20FB, chain A). The model was rebuilt using O [29]. The structure was refined by several rounds of positional, simulated annealing and individual B-factor refinements using CNS [30] followed by manual remodeling after each round of refinement. Statistics of data collection and refinement were shown in Table 2. All the structural figures were generated with Pymol (http://www.pymol.org).

# NMR spectroscopy

Uniform <sup>13</sup>C and <sup>15</sup>N labeling of MDA5 CTD was accomplished by growing E. Coli cells in minimal media supplemented with 2 g/L of [13C-6]-D-glucose and 1 g/L of 15NH<sub>4</sub>Cl (Cambridge Isotopes). All NMR experiments were carried out at 25 °C on Varian Inova spectrometers operating at <sup>1</sup>H Larmor frequencies of 500 and 600 MHz. Sequential assignments of the backbone <sup>1</sup>H, <sup>13</sup>Cα, <sup>13</sup>Cβ, and <sup>15</sup>N were obtained using gradient-enhanced CBCA(-CO)NH and HNCACB experiments [31]. NMR titration of MDA5 CTD with 10 bp dsRNA was carried out at 500 MHz. The protein concentration was maintained at 100 µM, while the concentration of 10 bp dsRNA was adjusted to 12, 30, 60, 120, and 240  $\mu$ M in a set of NMR samples. The binding of 10 bp dsRNA to MDA5 CTD was monitored using two-dimensional <sup>1</sup>H-<sup>15</sup>N HSQC spectra that correlate amide proton and nitrogen chemical shifts of the protein. NMR data were processed with nmrPipe [32] and assigned with Sparky 3 (http://www.cgl.ucsf.edu/home/sparky).

**Table 2**Data collection and refinement statistics.

	MDA5 CTD
Data collection	
Space group	P2 <sub>1</sub>
Cell dimensions	
a, b, c (Å)	28.41, 60.92, 36.44
α, β, γ (°)	90.00, 102.58, 90.00
Resolution (Å)	50-1.45 (1.50-1.45) <sup>a</sup>
R <sub>merge</sub>	3.9 (6.4)
<i>Ι</i> /σ <i>Ι</i>	64.5 (45.6)
Completeness (%)	94.2 (86.8)
Redundancy	4.3 (3.9)
Refinement	
Resolution (Å)	50-1.45
No. reflections	20278
R <sub>work</sub> / R <sub>free</sub>	18.0 / 20.4
No. atoms	
Protein	1091
Zinc ion	1
Water	204
B-factors	
Protein	15.42
Zinc ion	12.14
Water	28.3
R.M.S. deviations	
Bond lengths (Å)	0.010
Bond angles (°)	1.56

<sup>&</sup>lt;sup>a</sup> Values in parentheses are for highest-resolution shell.

Molecular modeling of the dsRNA/MDA5 complex

To generate the model, LGP2 CTD in the LGP2/dsRNA complex is superimposed on the MDA5 CTD structure using LSQKAB in the CCP4 suite [28] and the 8 bp dsRNA was replaced with a 12 bp dsRNA to show how MDA5 would interact with the first complete turn of the dsRNA. The loop connecting strands  $\beta$ 5 and  $\beta$ 6 was remodeled manually according to the LGP2/dsRNA complex structure using O [29]. The model was then optimized by energy minimization to eliminate close contact between the protein and the RNA using CNS [30].

#### Results

MDA5 CTD binds short dsRNA with blunt ends

Our previous studies on dsRNA recognition by LGP2 and RIG-I showed that dsRNA with blunt ends, but not dsRNA with 3' overhangs, are recognized by these two RLRs. To test whether MDA5 also recognizes dsRNA with blunt ends, we synthesized 8 bp dsRNA with blunt ends and with 5' or 3' overhangs and studied their binding with MDA5 by gel filtration chromatography (Table 1). As predicted, the 8 bp dsRNA with blunt ends binds MDA5 (Fig. 1A). We estimate that the stoichiometry between MDA5 CTD and the 8 bp dsRNA is likely to be 1:1 since the elution volume of the complex (16.8 ml) is smaller than that for the 2:1 complex of LGP2 CTD with the same dsRNA (15.7 ml) [25]. Furthermore, a short hairpin RNA containing only one blunt end also binds MDA5 CTD (Fig 1B). In contrast, the 8 bp dsRNA with either 5' or 3' overhangs does not bind MDA5 CTD (Fig. 1C and D). In addition, a 24 bp blunt-ended dsRNA also binds MDA5 CTD at slightly lower affinity compared to the 8 bp dsRNA. To test whether the 5' triphosphate group is need for RNA binding by MDA5, we generated ssRNA and dsRNA with 5' triphosphate group using RNA synthesized by in vitro transcription with T7 RNA polymerase and conducted binding studies with MDA5 CTD by gel filtration chromatography. The binding studies demonstrated that 5' ppp ssRNA does not interact with MDA5 CTD, but dsRNA with 5' triphosphate groups still binds the protein (Fig. 1E and F). These binding studies indicated that the blunt termini of dsRNA with or without phosphate groups are most likely the structural motif recognized by the MDA5. Since previous studies suggested that MDA5 specifically recognizes long dsRNA, We also tested whether long poly I:C associates with MDA5 CTD, but no binding was observed between MDA5 CTD and poly I:C.

To confirm that MDA5 CTD binds dsRNA with blunt ends, we also conducted RNA binding studies of MDA5 CTD by surface plasmon resonance (Table 1). We captured the 6× His-tagged or GST-tagged MDA5 CTD on sensor chips with immobilized anti-His or anti-GST antibodies. Clear binding signals were observed for an 8 bp 5' ppp dsRNA, a 24 bp dsRNA, and a hairpin RNA (Fig. 2). Analysis of the equilibrium binding data showed the 8 bp 5' ppp dsRNA, the 24 bp dsRNA, and the hairpin RNA bind MDA5 CTD at affinities  $(K_d)$  of  $5.7 \pm 0.3$ ,  $2.8 \pm 0.3$ , and  $2.3 \pm 0.2 \,\mu\text{M}$ , respectively (Fig. 2). The comparable affinities of MDA5 CTD for blunt-ended dsRNA and 5' ppp dsRNA indicates that the 5' triphosphates is not absolutely need for dsRNA binding. Since saturation of the binding reactions were not reached for the 24 bp dsRNA and the hairpin RNA, the  $K_d$  reported here are just estimations of the approximate binding affinities. The sensorgrams showed characteristics of fast kinetics for the association and dissociation reactions, indicating that electrostatic interactions may have played a key role in the interactions between MDA5 CTD and the dsRNAs. Although clear binding for

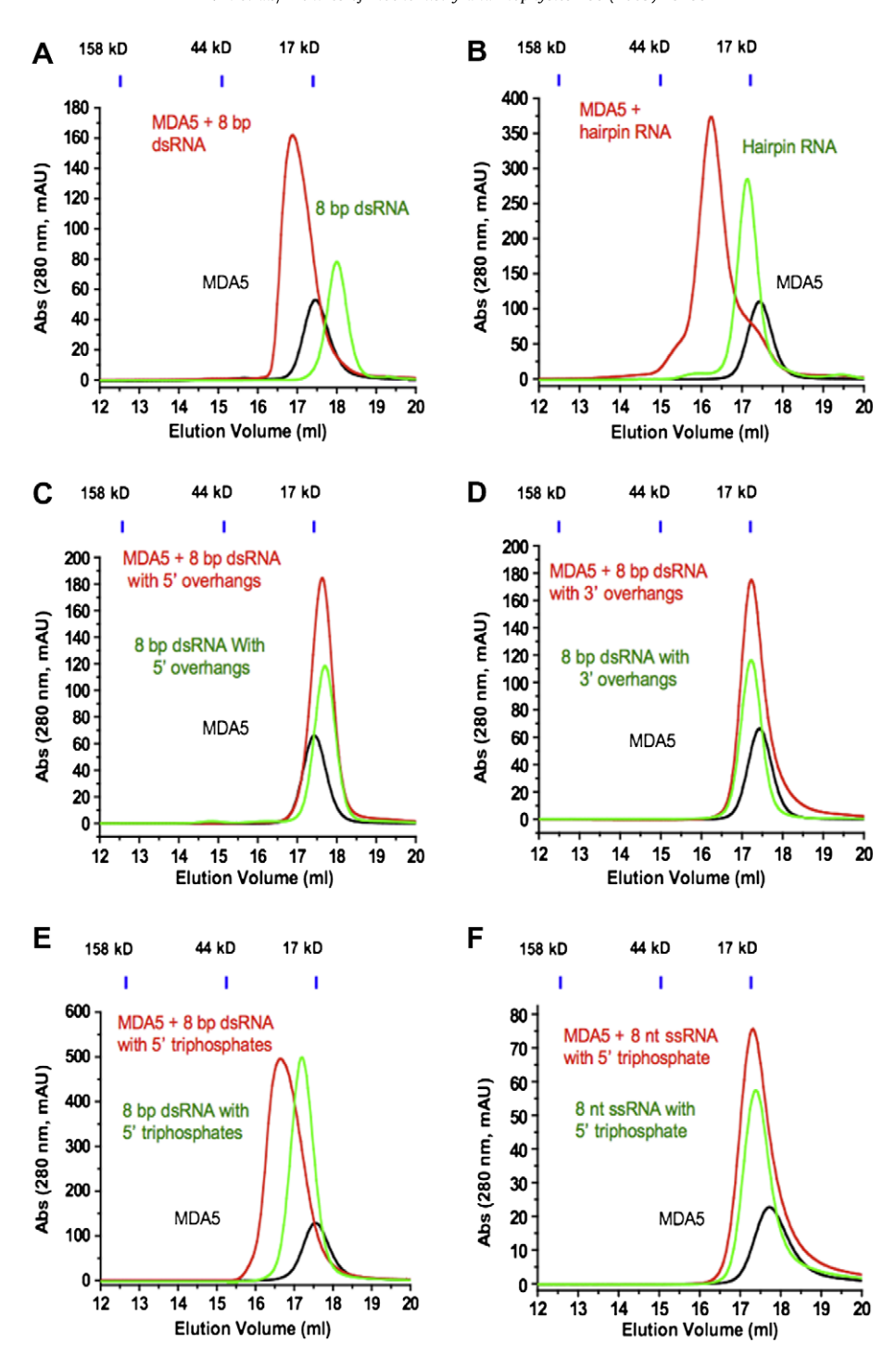


**Fig. 1.** MDA5 C-terminal domain binds dsRNA with blunt ends. (A) Gel filtration chromatography binding studies of MDA5 CTD and an 8 bp dsRNA with blunt ends. The elution volumes of three protein standards of molecular masses 158, 44 and 17 kDa are shown above the chromatogram. MDA5 CTD is shown by the black chromatogram, the dsRNA is shown by the green chromatogram, and the mixture of MDA5 CTD and dsRNA is shown by the red chromatogram. (B) Gel filtration chromatography binding study of MDA5 CTD with a 24-nucleotide hairpin RNA with one blunt end. (C) Binding studies of MDA5 CTD with an 8 bp dsRNA with two 3' overhanging nucleotides. (E). Binding studies of MDA5 CTD with an 8 bp dsRNA containing 5' triphosphates. (F). Binding studies of MDA5 CTD with an 8-nucleotide ssRNA containing 5' triphosphates.

the 8 bp dsRNA with blunt ends was observed in gel filtration chromatography, no binding signal was detected by SPR at concentration up to 100  $\mu M.$  In addition, no apparent binding was observed for 8 bp dsRNA with either 5' overhang or 3' overhang injected over the chip at concentrations of 10  $\mu M.$  Moreover, 5' ppp ssRNA of 8 and 22 nucleotides also showed no apparent binding by SPR at concentrations of 100  $\mu M.$ 

Crystal structure of MDA5 C-terminal domain

To understand the structural basis of dsRNA recognition by MDA5, we have crystallized MDA5 CTD (residues 892 to 1017 with a C-terminus  $6\times$  His tag) and determined its structure at 1.45 Å resolution (Fig. 3A). Deletion of residues 1018–1025 containing Cys1018 and 1019 at the C-terminus of MDA5 was crucial for the

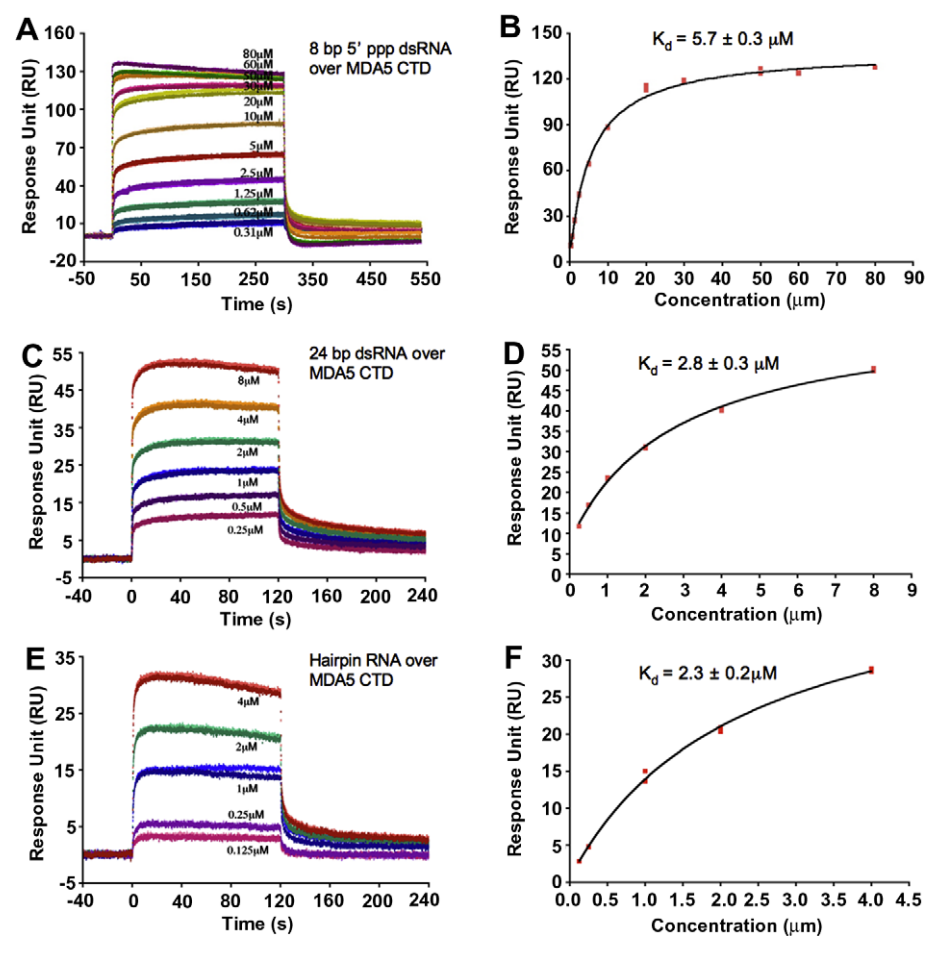


**Fig. 2.** RNA binding studies of MDA5 CTD by surface plasmon resonance (SPR). In the equilibrium binding studies, serial dilutions of different forms of RNAs were injected over sensor chips with MDA5 CTD captured by immobilized anti-GST or anti-His antibodies. Double-reference subtracted sensorgrams are shown for an 8 bp dsRNA with 5′ triphosphates (A), a 24 bp dsRNA (C), and a 24 nucleotide hairpin RNA (E). The corresponding binding analyzes are shown in (B) (for the 8 bp dsRNA with 5′ triphosphates), (D) (for the 24 bp dsRNA), and (F) (for the hairpin RNA). The equilibrium binding constants ( $K_d$ ) are derived from global fitting of the data to a one-site binding model.

crystallization of MDA5 CTD by preventing the formation of non-homogenous dimers at high-protein concentration. All the residues of MDA5 CTD except residues Asn993 to Thr996 are well defined in the electron density map.

The structure of MDA5 CTD revealed a highly conserved fold similar to the structures of the CTDs of RIG-I and LGP2 [16,22,24]. MDA5 CTD contains a four-stranded ( $\beta$ 1,  $\beta$ 2,  $\beta$ 9 and  $\beta$ 10) antiparallel  $\beta$ -sheet near its N-terminus and another fourstranded ( $\beta$ 5,  $\beta$ 6,  $\beta$ 7 and  $\beta$ 8) antiparallel  $\beta$ -sheet in the middle (Fig. 3A). The two  $\beta$ -sheets are connected by a  $\beta$ -hairpin formed by strands  $\beta 3$  and  $\beta 4$  and a short  $\alpha$ -helix  $\alpha 1$ . Four conserved cysteine residues, Cys907, Cys910, Cys962 and Cys964, in the two loops connecting strands  $\beta1-\beta2$  and  $\beta6-\beta7$  make additional connection between the two  $\beta$ -sheets by coordinating a zinc ion (Fig. 3A). The four cysteine residues are arranged tetrahedrally around the zinc ion and the distances between the sulfur atoms in the thiol groups and zinc atom are about 2.35 Å. It is evident this zinc ion plays a crucial role in maintaining the overall fold of MDA5 CTD; mutations of these residues in RIG-I abrogate its response to RNA in vivo [24]. Residues Tyr1015 to Glu1017 of MDA5 together with the  $6 \times$  His tag form a short helix  $\alpha 2$  (Fig. 3A).

The solution structure of MDA5 CTD was determined by NMR spectroscopy recently [33]. Superposition of one representative NMR structure with the crystal structure shows the solution structure is close to the crystal structure with a rmsd of 1.4 Å for 111 C $\alpha$  atoms and 1.9 Å for all atoms in these 111 residues. Major differ-

ences between the two structures occur at the N-terminus, the C-terminus, and the loop between strand  $\beta 5$  and  $\beta 6$ . The solution structure shows these regions of the protein are flexible. The inclusion of residues Cys1018 to Asp1025 in the sample for NMR studies has no significant effect on the overall structure of MDA5 CTD in solution.

Although the amino acid sequence of MDA5 CTD is only 24.3% and 29.5% identical to the CTDs of RIG-I and LGP2, the structures of the three proteins are highly conserved, reflecting their conserved roles in dsRNA binding. The rmsd between the 104  $C\alpha$ atoms in MDA5 and LGP2 CTDs is only 1.15 Å (Fig. 3B). The structures of MDA5 and RIG-I CTDs are very similar as well; the rmsd between 101 conserved  $C\alpha$  atoms in the two proteins is only 1.14 Å (Fig. 3C). The major structural differences between these proteins occur at the long loop (loop 5-6) connecting strands β5 and β6 (Fig. 3B and C). The crystal structure of LGP2 CTD/dsRNA complex indicated that this loop is involved in the interactions between the blunt termini of dsRNA and LGP2 [25]. The conformation of this loop in MDA5 CTD is ordered and similar to the crystal structure of this loop in RIG-I [24], but is different from the corresponding loop in LGP2 in the LGP2/dsRNA complex structure (Fig. 3B and C). Structural studies of RIG-I CTD by NMR spectroscopy and LGP2 CTD in isolation by crystallography indicated this loop is flexible [16,22]. It is most likely dsRNA binding induces a large conformational change in this loop to facilitate the interactions between the termini of dsRNA and RLRs. The defined

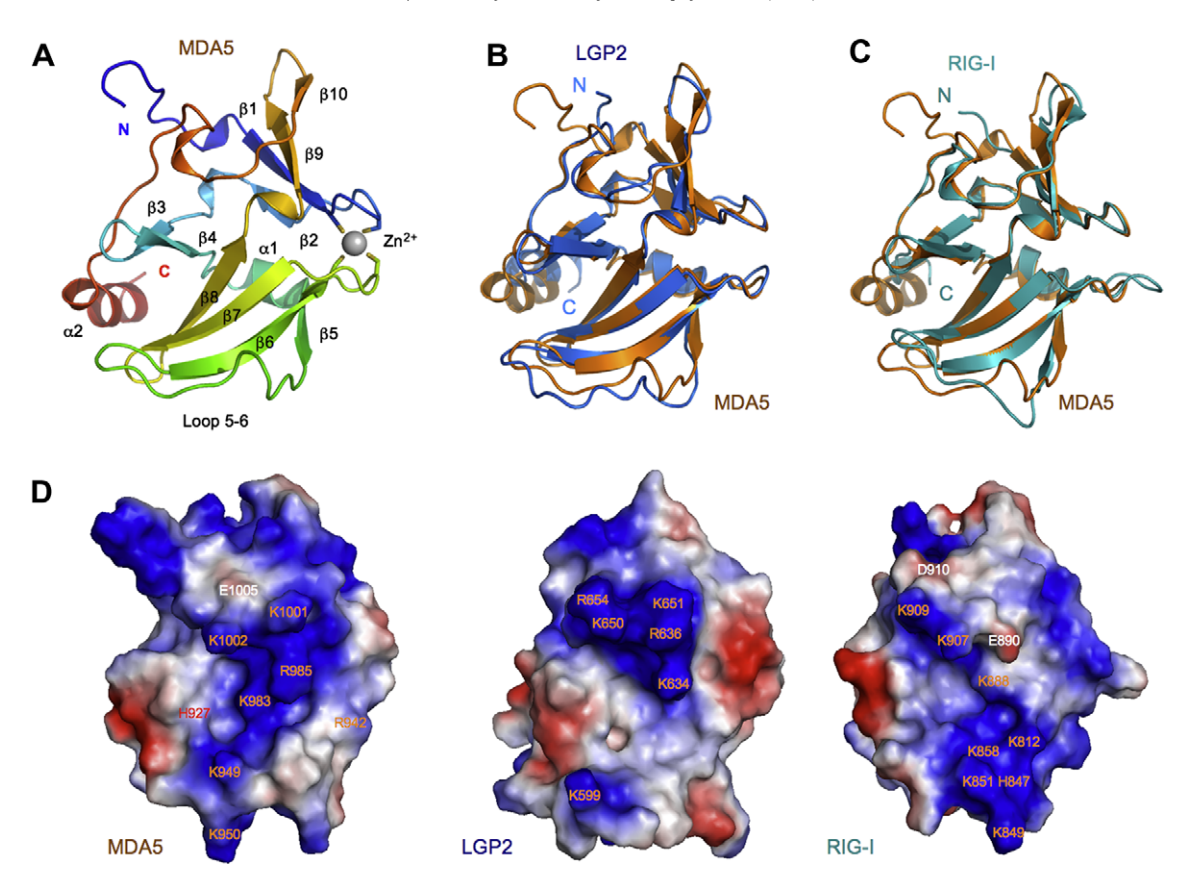


**Fig. 3.** Crystal structure of human MDA5 CTD and comparison with the structures of LGP2 and RIG-I CTDs. (A) Ribbon representation of the structure of MDA5 CTD. The protein molecule is colored rainbow from blue at the N-terminus to red at the C-terminus. The zinc ion is shown by the gray sphere and sidechains of four cysteine residues coordinating with the zinc ion are shown by stick models. (B) Superposition of the structures of MDA5 CTD and LGP2 CTD. The LGP2 CTD structure is derived from the LGP2 CTD/dsRNA complex structure with its dsRNA binding surface facing the reader. (C) Superposition of the structures of MDA5 CTD and RIG-I CTD. (D) Comparison of the surface electrostatic potential of the CTDs of MDA5, LGP2 and RIG-I. The orientation of the MDA5 CTD is the same as in panel A. LGP2 and RIG-I CTDs are oriented the same way as MDA5 CTD with their RNA binding surfaces facing the reader. The potential 5' triphosphates binding site of RIG-I CTD is at the positively charged patch of residues around Lys858.

structure of loop 5–6 in the MDA5 CTD structure is stabilized by crystal packing contacts.

Based on the structure of LGP2/dsRNA complex [25], we predict that the surface defined by the  $\beta$ -sheet containing  $\beta$ 5 to  $\beta$ 8, the  $\beta$ hairpin, and the three loops connecting  $\beta 5-\beta 6$ ,  $\beta 8-\beta 9$ , and  $\beta 9$  to the C-terminal helix in MDA5 is likely involved in dsRNA binding. Examination of this potential RNA binding surface showed that it is positively charged and exhibits a high degree of shape complementarity to the structure dsRNA (Fig. 3D). However, the surface electrostatic potential of the three proteins are quite different (Fig. 3D), reflecting their different roles in viral RNA sensing. Although the surface of RIG-I CTD is also highly positively charged and the shape of the RNA binding surface is similar to that of LGP2 and MDA5, there is an extra patch of positively charged surface around residues Lys858, Lys851 and Lys861 (Fig. 3D). This positively charged surface is likely involved in the recognition of the 5' triphosphate group of ssRNA or dsRNA [22,24]. Mutations of residues Lys858 and 861 to alanine at the same time at this surface abolished 5' ppp ssRNA binding signaling by RIG-I [22]. Mutations of Lys858, Lys888 or His830 to negatively charged glutamate residues abrogated the response of RIG-I to ssRNA with 5' triphosphates [24].

Identification of the dsRNA binding surface of MDA5 CTD by NMR spectroscopy

Excellent chemical shift dispersion of the ligand-free MDA5 CTD  $^1\mathrm{H-^{15}N}$  HSQC spectrum (Fig. 4A) has made it possible to identify

the dsRNA binding surface of MDA5 CTD. For the majority of residues that are involved in or perturbed by protein–dsRNA interaction, the kinetics of dsRNA binding to MDA5 CTD falls into an intermediate exchange regime on the NMR chemical shift timescale, resulting in broadening and gradual disappearance of cross-peaks with increasing ligand concentration. Even at low concentration of the dsRNA, 12  $\mu M$ , the effect of ligand binding was noticeable for the 21 residues whose cross-peaks are labeled in the NMR spectrum (Fig. 4A). At each concentration of dsRNA up to 60  $\mu M$ , we identified the protein residues whose cross-peaks disappeared, or significantly changed their intensity and/or chemical shift compared to the ligand-free protein. The results of this analysis are summarized in Fig. 4B.

Most of the residues with reduced intensity in the spectra are located on the hairpin containing strands  $\beta 3$  and  $\beta 4$ , the loop connecting  $\beta 5$  and  $\beta 6$ , the strands  $\beta 7$  and  $\beta 8$ , the loop connecting  $\beta 8$  and  $\beta 9$ , and the loop connecting strands  $\beta 10$  to the C-terminal helix (Fig. 4B and C). Obviously, these residues are mapped on the surface of MDA5 that corresponds to the dsRNA binding surface of RIG-I and LGP2 identified by NMR titration of RIG-I and the crystal structure of the LGP2 CTD/dsRNA complex (Fig. 4C). These results indicate that all the RLRs use a highly conserved positively charge surface to bind dsRNA. Since the overall structure of MDA5 CTD is very similar to LGP2 CTD, it is likely MDA5 also binds to the blunt ends of dsRNA in a similar manner as LGP2. As observed in RNA binding studies of RIG-I CTD by NMR [22], only a few residues on the opposite surface

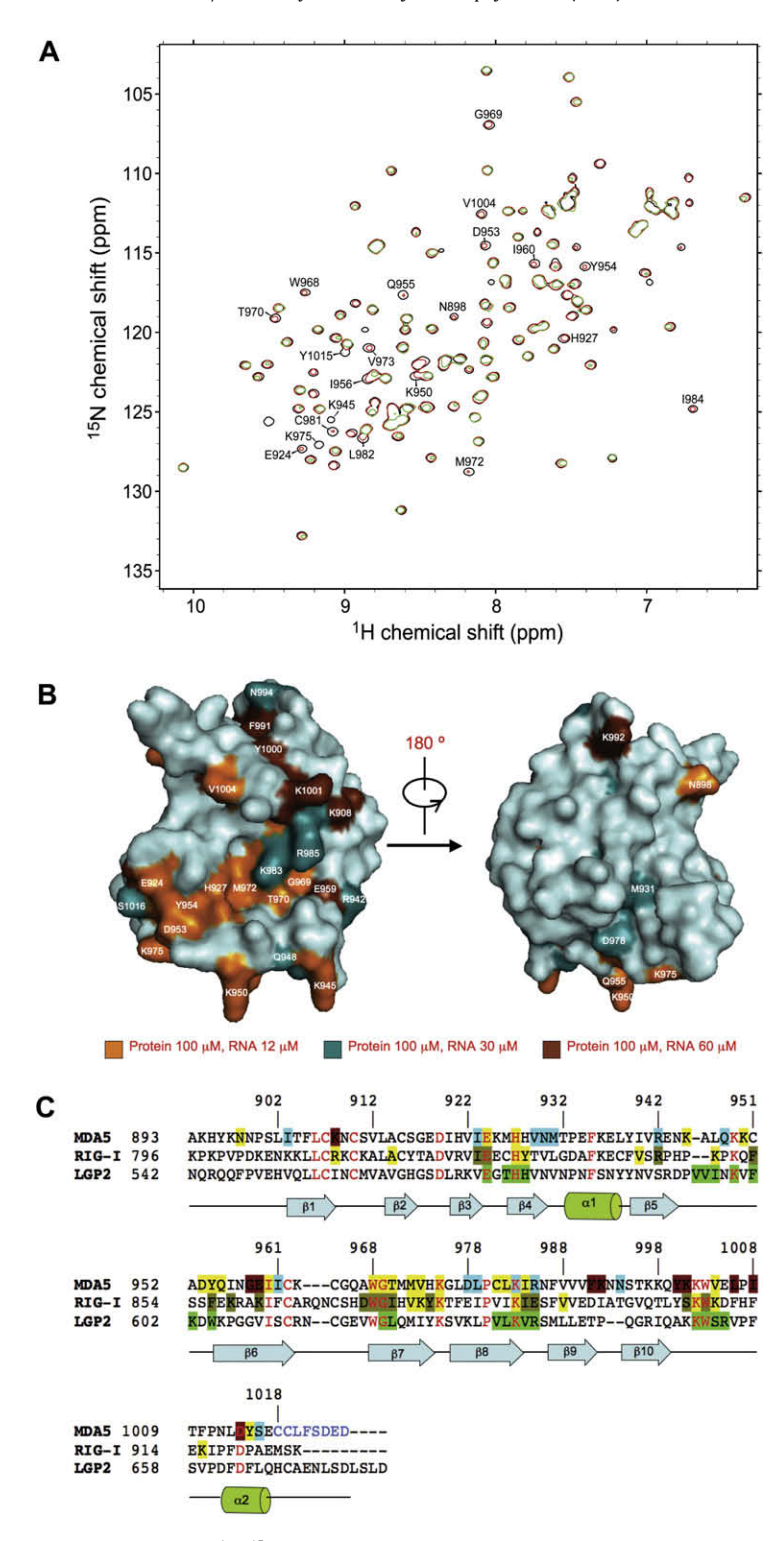


**Fig. 4.** The dsRNA binding surface of MDA5 CTD. (A) 500 MHz <sup>1</sup>H-<sup>15</sup>N HSQC spectra of 100 μM MDA5 CTD in the presence of 0 μM (black), 12 μM (red), and 30 μM (green) dsRNA. Cross-peaks whose intensity decreased in response to adding 12 μM dsRNA are labeled. (B) Mapping of amino acid residues involved in dsRNA binding identified by NMR spectroscopy onto the crystal structure of MDA5 CTD. Residues involved in RNA binding at RNA concentrations of 12 μM, 30 μM, and 60 μM and protein concentration of 100 μM are colored orange, teal, and chocolate, respectively. (C) Structure-based sequence alignment of human MDA5, RIG-I and LGP2 CTDs. Conserved residues in the three proteins are shown in red. Residues of MDA5 not included in the protein for crystallization are shown in light blue. Secondary structural elements of MDA5 CTD are shown under the aligned sequences. Residues of MDA5 involved in dsRNA binding at concentrations of 12 μM, 30 μM, and 60 μM and protein concentration of 100 μM are highlighted in yellow, cyan, and chocolate, respectively. NMR titration of RIG-I CTD identified an overlapping sets of residues are involved in dsRNA and 5′ ppp ssRNA. Residues of RIG-I CTD involved in dsRNA are highlighted in yellow; residues involved in 5′ ppp ssRNA recognition in addition to those residues that are involved in dsRNA binding observed in the crystal structure of the LGP2 CTD/dsRNA complex are highlighted in green. (For interpretation of color mentioned in this figure the reader is referred to the web version of the article.)

of MDA5 CTD showed significant changes in intensity or chemical shift upon dsRNA binding (Fig. 4B). In addition, a number of

residues near the dsRNA binding surface but do not contact the dsRNA directly also showed reduced intensity in presence of dsRNA, indicating global conformational adjustment of MDA5 CTD might be involved in dsRNA binding.

HSQC spectra of MDA5 CTD-dsRNA complexes collected at  $120~\mu M$  and  $240~\mu M$  dsRNA concentrations are virtually indistinguishable, indicating full saturation of protein with ligand. Even at saturating concentrations of dsRNA we observed significant line-broadening of NMR cross-peaks that cannot be fully explained by an increase in molecular weight due to the protein–dsRNA complex formation. One plausible explanation is the formation of 2:1 complex between MDA5 CTD and the dsRNA at higher concentrations, which increases the molecular weight of the complex significantly.

Electrostatic interactions play primary roles in dsRNA recogniton by MDA5

The structure of LGP2 CTD/dsRNA complex revealed that LGP2 interacts with dsRNA primarily through electrostatic interactions between the phosphate backbone and positively charged residues [25]. The blunt ends of the dsRNA interact with LGP2 through hydrogen bonds and hydrophobic interactions. Based on the structural comparison of MDA5 CTD and the LGP2 CTD/dsRNA complex structures, we generated seven mutants of MDA5 CTD and studied their binding properties with an 8 bp dsRNA by gel filtration chromatography (Fig. 5). These binding studies demonstrated that

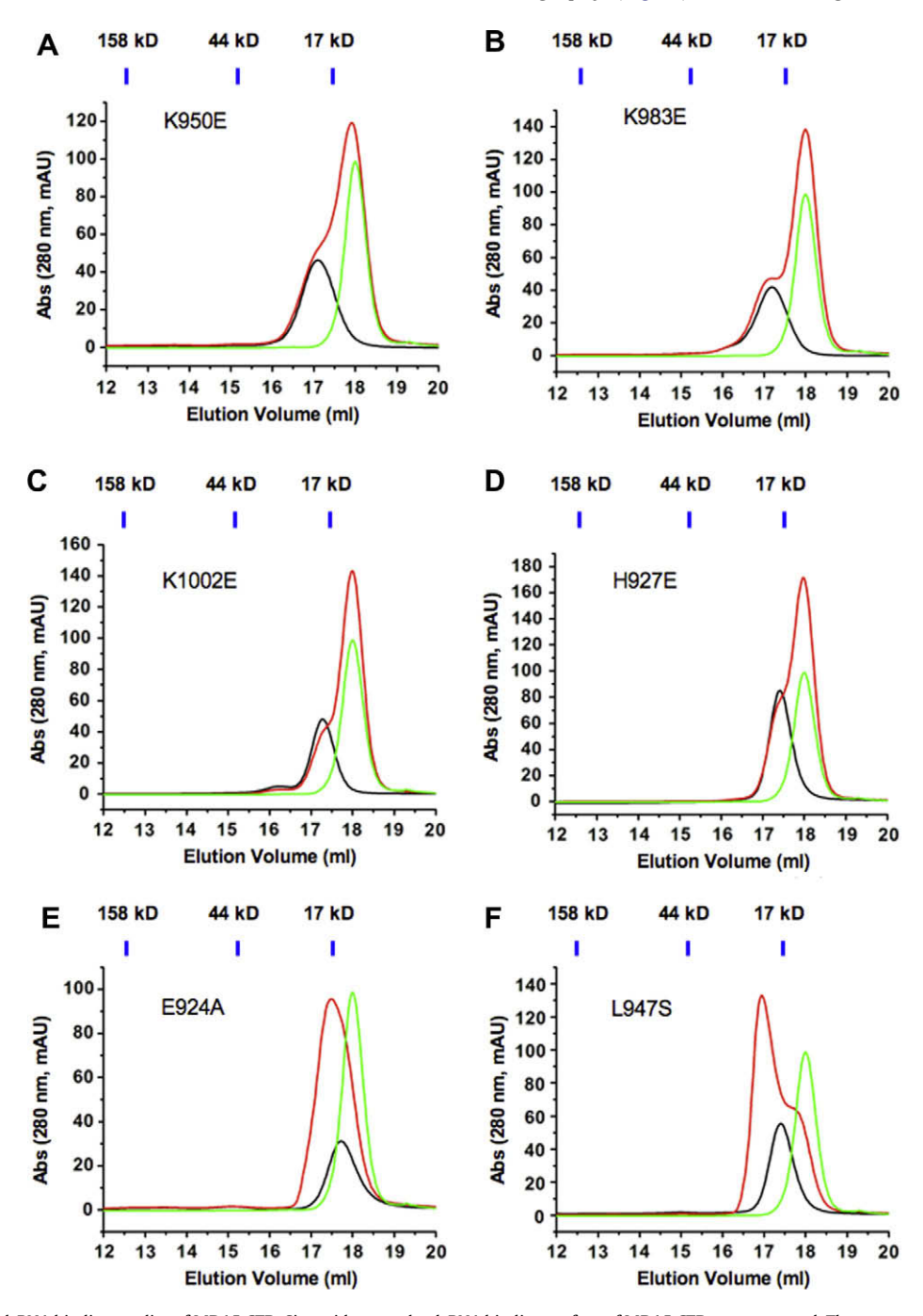


**Fig. 5.** Mutagenesis and dsRNA binding studies of MDA5 CTD. Six residues on the dsRNA binding surface of MDA5 CTD were mutated. The mutant proteins were purified and their binding for an 8 bp dsRNA were studied by gel filtration chromatography. The dsRNA are shown by the green chromatograms, MDA5 CTD mutants by the black chromatograms, and the mixtures of MDA5 CTD and the dsRNA by the red chromatograms. The elution volumes of three protein standards of molecular masses 158, 44, and 17 kDa are shown above the chromatogram. Mutations of each of the four residues K950, K983, K1002 or H927 to negatively charged glutamate residues (A to D) abolished dsRNA binding, while mutants of E924A (E) and L947S (F) retained dsRNA binding activity.

mutations of any one of the three positively charged residues Lys950, Lys983 and Lys1002 to negatively charged glutamate residues abolished dsRNA binding by MDA5 CTD (Fig. 5A-C), indicating these residues play primary roles in dsRNA recognition by MDA5. Mutation of the two lysine residues that correspond to Lys983 and Lys1002 of MDA5 in RIG-I and LGP2 CTD also disrupted RNA binding by RIG-I and LGP2 [22,25], demonstrating these two conserved lysine residues play pivotal roles in dsRNA recognition by the RLRs. As a control, mutation of Arg942, a residue that is not on the predicted dsRNA binding surface of MDA5, to glutamate did not affect dsRNA binding (data not shown). In addition, mutation of the conserved histidine residue His927 that is involved in the formation of a network of hydrogen bonds in LGP2 CTD/dsRNA complex to glutamate also disrupted dsRNA binding by MDA5 CTD (Fig. 5D), indicating this residue plays important roles in dsRNA binding. As observed in the mutagenesis analysis of LGP2 CTD [25], mutation of Glu924 to alanine or Leu947 to serine, two residues that might ineract with dsRNA by hydrogen bond and hydrophobic interactions, do not abrogate dsRNA binding by MDA5 CTD (Fig. 5E and F), suggesting these two residues might contribute to dsRNA binding but do not play dominant roles in dsRNA recognition. Since the affinity of MDA5 CTD for dsRNA is lower than LGP2 CTD, a comparison of the two structures revealed that the replacement of Arg654 in LGP2 that interacts with the phosphate backone of dsRNA directly by Glu1005 in MDA5 is likely to be responsible for the significantly reduced affinity of MDA5 for dsRNA.

#### Molecular model of MDA5 CTD bound to dsRNA

Since the structures of the CTDs of the RLRs are highly conserved and similar positively charged surfaces are involved in dsRNA binding by all the three proteins, it is most likely they bind to the terminus of dsRNA in a similar way as observed in the LGP2 CTD dsRNA complex structure. To understand how MDA5 CTD binds dsRNA, we have generated a structural model of MDA5 CTD bound to a 12 bp dsRNA based on the LGP2/dsRNA complex structure [25], the MDA5/dsRNA binding surface identified by NMR titration, and results from the mutagenesis and RNA binding studies of MDA5 CTD (Fig. 6A and B). The model was generated by superposition of the MDA5 CTD structure on the LGP2 CTD structure in the LGP2/dsRNA complex. The 8 bp dsRNA in the LGP2/ dsRNA complex was replaced by a 12 bp dsRNA to show how MDA5 might interact with the first complete turn of the dsRNA. The model was optimized by manual remodeling and energy minimization. Except for the major structural adjustment of the loop connecting \$5 and \$6 based on the structure of this loop in the LGP2 CTD/dsRNA complex structure, minor structural adjustment of the overall structure of MDA5 CTD is required to accommodate the dsRNA. The rmsd between all the 125  $C\alpha$  atoms in the optimized model and the native MDA5 structure is only 1.57 Å, while the rmsd between 115 C $\alpha$  atoms (not including the 10 C $\alpha$  atoms in loop 5–6) in the model and native MDA5 CTD is only 0.65 Å. Like LGP2 CTD, MDA5 CTD in the model shows a high degree of charge and shape complementarity to the first turn of dsRNA (Fig. 6C).

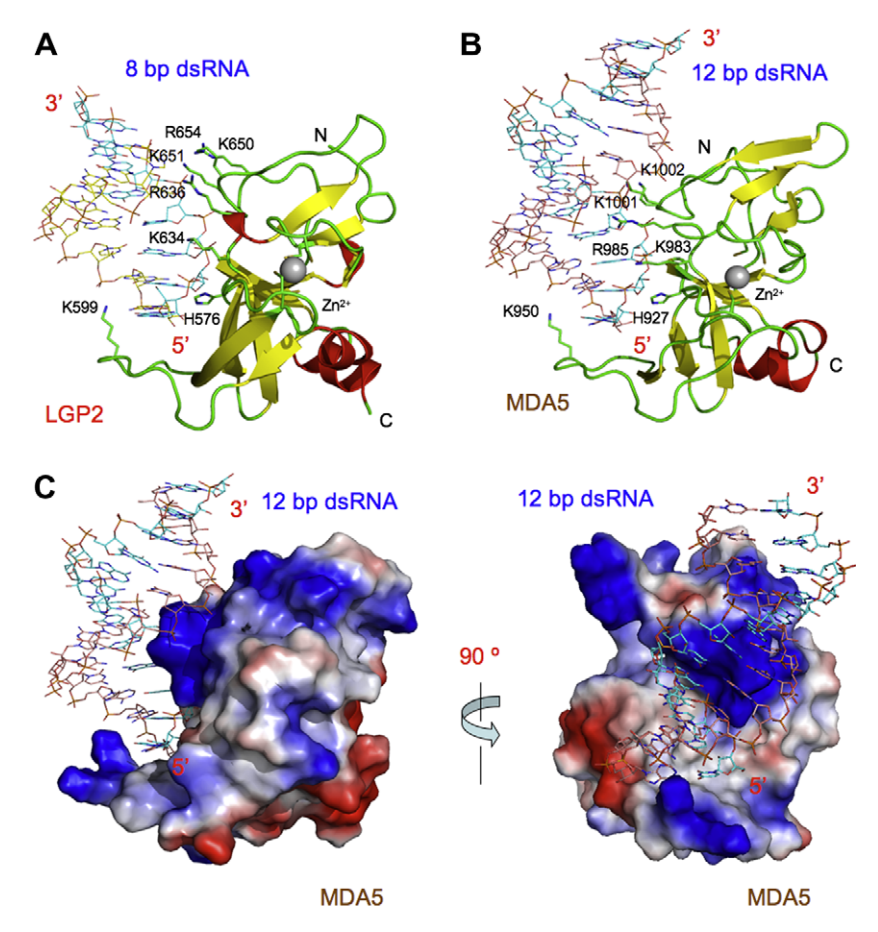


**Fig. 6.** Structural model of MDA5 CTD bound to dsRNA. (A) Crystal structure of human LGP2 CTD bound to an 8 bp dsRNA. The dsRNA is shown in stick models. Sidechains of critical residues involved in RNA binding by MDA5 are shown in stick models and labeled. The zinc ion is shown as gray sphere with cysteine residues coordinating with it shown as stick models. (B) Structural model of MDA5 CTD bound to a 12 bp dsRNA. (C) Surface representation of the MDA5 CTD bound to a 12 bp dsRNA in two different orientations. The orientation of MDA5 CTD on the left image has the same orientation as MDA5 CTD in B. MDA5 CTD is colored by its surface electrostatic potential (ranging from blue = 10 kT/e to red = -10 kT/e).

The MDA5 CTD/dsRNA complex model (Fig. 6B) showed that four positively charged residues, Lys983, Arg985, Lys1001, and Lys1002, in the two loops connecting  $\beta 8$  to  $\beta 9$ , and  $\beta 9$  to the C-terminal helix would interact with the phosphate backbone of the first turn of the dsRNA through extensive electrostatic interactions. The two conserved lysine residues Lys1001 and Lys1002 would reach into the major grove of the dsRNA and may interact with the phosphate groups of the fifth nucleotide near the 3' end of one RNA strand and the ninth nucleotide at the 5' end of the other strand (Fig. 6B). Residues Lys983 and Arg985 might make additional electrostatic interactions with the phosphate group of the second and third nucleotides near the 5' end and the eighth nucleotide near the 3' end of the dsRNA. All of these positively charged residues are conserved in the sequences of MDA5 and LGP2 and are likely to interact with dsRNA in similar ways (Fig. 4C). The loop connecting strands 65 and 66 was completely remodeled so that it would wrap around the end of the dsRNA and interact with the RNA through extensive hydrophobic interactions and hydrogen bonds as observed in the LGP2/dsRNA complex structure. Additional details about how MDA5 CTD binds dsRNA await the determination of the crystal structure of MDA5 bound to dsRNA.

#### Discussion

RNA binding studies by gel filtration chromatography and SPR demonstrated that MDA5 CTD only binds dsRNA with blunt ends, but does not associate with dsRNA with either 5' or 3' overhangs. These results confirmed previous findings that MDA5 is a sensor of dsRNA. Similar preferences of blunt-ended dsRNA were also observed for the LGP2 and RIG-I CTD, indicating the blunt end of dsRNA is most likely a common structural motif recognized by the RLRs [25]. The CTD of MDA5 exhibits significantly lower affinities for dsRNA ( $K_d \sim 3 \ \mu M$ ) compared to the CTD of LGP2 ( $K_d \sim 100 \ nM$ ) [25] and RIG-I ( $K_d \sim 340$  nM, P.L. unpublished data) suggesting MDA5 needs higher concentrations of ligands for activation. RNA binding studies of full-length LGP2 and the CTD of LGP2 showed that the affinity of CTD is comparable to the full-length protein, indicating the CTD plays primary roles in RNA binding [25,34]. In addition, the affinities of full-length and the CTD of RIG-I to 5' ppp ssRNA are also comparable to each other ( $K_d \sim 150 \text{ nM}$  and  $\sim 220 \text{ nM}$ ) [24]. Based on these findings, it is likely the CTD of MDA5 also plays a key role in dsRNA binding. Since MDA5 CTD has lower affinities for dsRNA, it formed a 1:1 complex with 10 bp dsRNA at low concentration and a mixture of 1:1 and 2:1 complexes at higher concentration, making the MDA5/dsRNA complex heterogeneous and resistant to

The structure of MDA5 CTD revealed a highly conserved fold similar to the CTD of RIG-I and LGP2 (Fig. 3B and C). All the three proteins show a high degree of shape and charge complementarity with the first turn of blunt-ended dsRNA. Consistent with this, NMR titration of MDA5 CTD with dsRNA indicated that a conserved positively charged surface is involved in dsRNA binding. Structural studies of RIG-I CTD by NMR spectroscopy and LGP2 CTD in complex with dsRNA by crystallography indicated that a similar binding surface is involved in dsRNA and ssRNA binding by RIG-I and dsRNA binding by LGP2 [22,25]. Molecular modeling of MDA5 CTD/dsRNA complex indicates that it is most likely MDA5 CTD binds to the first turn of blunt-ended dsRNA in a similar way as LGP2 CTD. Mutagenesis and RNA binding studies of MDA5, RIG-I, and LGP2 CTD demonstrated that electrostatic interactions mediated by a set of conserved positively charged residues corresponding to Lys983 and Lys1002 in MDA5 play critical roles in dsRNA recognition by all three proteins [16,22,24,25]. Since several mutants of MDA5 with abolished dsRNA binding were identified in this study, it will be interesting to test whether these mutants of MDA5 still stimulate type I IFN induction in virus infected cells. These studies will provide insight into whether the dsRNA binding is needed for MDA5 signaling. Since the coexpression of LGP2, which exhibits much higher affinities for dsRNA than MDA5, stimulated rather than suppressed the activation of MDA5 [16], the roles of dsRNA binding in MDA5 activation need to be reconsidered. It is also possible that dsRNA binding is not required for the regulation of MDA5 by LGP2. Previous studies from two independent groups already showed that mutants of LGP2 with abolished RNA binding still suppress the activation of RIG-I [25,35].

RNA binding studies clearly showed MDA5 CTD also binds short dsRNA of 8 to 24 bp in length just like the CTD of LGP2 and RIG-I. Since the affinity of MDA5 CTD for blunt-ended dsRNA is only about 3 µM, it is difficult to understand why full-length MDA5 prefers long dsRNA instead of short dsRNA as ligands, since the concentration of the blunt ends, the structural motif of dsRNA recognized by MDA5, would be very low for a given amount of long dsRNA. For example, a solution of a 2 kb dsRNA at 3 µM concentration corresponds to a solution of 20 bp dsRNA at 300 µM concentration with the same amount of RNA. On the other hand, the maximum length of dsRNA that can be covered by a full-length MDA5 molecule is likely about 30 bp assuming the maximum dimension of the molecule is about 100 Å as observed in the electron microscopy structure of full-length LGP2 and RIG-I [34,36]. Moreover, our previous studies demonstrated that 24 bp but not 19 bp dsRNA stimulates the activation of RIG-I, indicating that the 24 bp dsRNA is long enough to form an active complex with full-length RIG-I [25]. The activation of antiviral ribonuclease, RNase L, by 2',5'-linked oligoadenylate (2-5A) produces small RNA cleavage products that initiate IFN production [37]. This is likely a mechanism to generate a large amount of short dsRNA to simulate the activation of the RLRs. However, it is not clear whether the products of RNase L serve as ligands for MDA5. The mechanism of how MDA5 is selectively activated by long dsRNA and poly I:C needs further investigation.

# Acknowledgment

This research is supported in part by a Grant from the Robert Welch Foundation (Grant No. A-1687) to P. Li.

Accession codes: The atomic coordinates and structure factors of MDA5 CTD have been deposited with the RCSB Protein Data Bank under accession code 3GA3.

#### References

- 1] S. Akira, S. Uematsu, O. Takeuchi, Cell 124 (2006) 783-801.
- [2] C.A. Janeway Jr., R. Medzhitov, Annu. Rev. Immunol. 20 (2002) 197-216.
- [3] A.N. Theofilopoulos, R. Baccala, B. Beutler, D.H. Kono, Annu. Rev. Immunol. 23 (2005) 307–336.
- [4] K. Honda, A. Takaoka, T. Taniguchi, Immunity 25 (2006) 349–360.
- [5] D.B. Stetson, R. Medzhitov, Immunity 25 (2006) 373-381.
- [6] T. Kawai, S. Akira, Ann. NY Acad. Sci. 1143 (2008) 1-20.
- [7] Y. Kumagai, O. Takeuchi, S. Akira, J. Infect. Chemother. 14 (2008) 86-92.
- [8] A.J. Thompson, S.A. Locarnini, Immunol. Cell. Biol. 85 (2007) 435-445.
- [9] M. Yoneyama, M. Kikuchi, T. Natsukawa, N. Shinobu, T. Imaizumi, M. Miyagishi, K. Taira, S. Akira, T. Fujita, Nat. Immunol. 5 (2004) 730–737.
- [10] O. Takeuchi, S. Akira, Curr. Opin. Immunol. 20 (2008) 17–22.
- [11] M. Yoneyama, T. Fujita, J. Biol. Chem. 282 (2007) 15315-15318.
- [12] E. Meylan, J. Tschopp, M. Karin, Nature 442 (2006) 39-44.
- [13] M. Yoneyama, T. Fujita, Immunity 29 (2008) 178–181.
- [14] S. Rothenfusser, N. Goutagny, G. DiPerna, M. Gong, B.G. Monks, A. Schoenemeyer, M. Yamamoto, S. Akira, K.A. Fitzgerald, J. Immunol. 175 (2005) 5260–5268.
- [15] M. Yoneyama, M. Kikuchi, K. Matsumoto, T. Imaizumi, M. Miyagishi, K. Taira, E. Foy, Y.M. Loo, M. Gale Jr., S. Akira, S. Yonehara, A. Kato, T. Fujita, J. Immunol. 175 (2005) 2851–2858.
- [16] D.A. Pippig, J.C. Hellmuth, S. Cui, A. Kirchhofer, K. Lammens, A. Lammens, A. Schmidt, S. Rothenfusser, K.P. Hopfner, Nucleic Acids Res. 37 (2009) 2014–2025.

- [17] H. Kato, O. Takeuchi, S. Sato, M. Yoneyama, M. Yamamoto, K. Matsui, S. Uematsu, A. Jung, T. Kawai, K.J. Ishii, O. Yamaguchi, K. Otsu, T. Tsujimura, C.S. Koh, C. Reis e Sousa, Y. Matsuura, T. Fujita, S. Akira, Nature 441 (2006) 101–105
- [18] L. Gitlin, W. Barchet, S. Gilfillan, M. Cella, B. Beutler, R.A. Flavell, M.S. Diamond, M. Colonna, Proc. Natl. Acad. Sci. USA 103 (2006) 8459–8464.
- [19] V. Hornung, J. Ellegast, S. Kim, K. Brzozka, A. Jung, H. Kato, H. Poeck, S. Akira, K.K. Conzelmann, M. Schlee, S. Endres, G. Hartmann, Science 314 (2006) 994– 997
- [20] A. Pichlmair, O. Schulz, C.P. Tan, T.I. Naslund, P. Liljestrom, F. Weber, C. Reis e Sousa, Science 314 (2006) 997–1001.
- [21] A. Pichlmair, C. Reis e Sousa, Immunity 27 (2007) 370-383.
- [22] K. Takahasi, M. Yoneyama, T. Nishihori, R. Hirai, H. Kumeta, R. Narita, M. Gale Jr., F. Inagaki, T. Fujita, Mol. Cell 29 (2008) 428–440.
- [23] H. Kato, O. Takeuchi, E. Mikamo-Satoh, R. Hirai, T. Kawai, K. Matsushita, A. Hiiragi, T.S. Dermody, T. Fujita, S. Akira, J. Exp. Med. 205 (2008) 1601–1610.
- [24] S. Cui, K. Eisenacher, A. Kirchhofer, K. Brzozka, A. Lammens, K. Lammens, T. Fujita, K.K. Conzelmann, A. Krug, K.P. Hopfner, Mol. Cell 29 (2008) 169–179.
- [25] X. Li, C.T. Ranjith-Kumar, M.T. Brooks, S. Dharmaiah, A.B. Herr, C. Kao, P. Li, J. Biol. Chem. 284 (2009) 13881–13891.
- [26] D.G. Myszka, J. Mol. Recognit. 12 (1999) 279-284.

- [27] Z. Otwinowski, W. Minor, Methods Enzymol. 276 (1997) 307-326.
- [28] CCP4, Acta Crystallogr. D Biol. Crystallogr. 50 (1994) 760–763.
- [29] T.A. Jones, M. kjeldgaard, Methods Enzymol. 277 (1997) 173-208.
- [30] A.T. Brunger, P.D. Adams, G.M. Clore, W.L. DeLano, P. Gros, R.W. Grosse-Kunstleve, J.S. Jiang, J. Kuszewski, M. Nilges, N.S. Pannu, R.J. Read, L.M. Rice, T. Simonson, G.L. Warren, Acta Crystallogr. D Biol. Crystallogr. 54 (1998) 905–921.
- [31] R.K. Muhandiram, L.E., J. Magn. Reson. Ser. B 103 (1994) 203-216.
- [32] F. Delaglio, S. Grzesiek, G.W. Vuister, G. Zhu, J. Pfeifer, A. Bax, J. Biomol. NMR 6 (1995) 277–293.
- [33] K. Takahasi, H. Kumeta, N. Tsuduki, R. Narita, T. Shigemoto, R. Hirai, M. Yoneyama, M. Horiuchi, K. Ogura, T. Fujita, F. Inagaki, J. Biol. Chem. 284 (2009) 17465–17474.
- [34] A. Murali, X. Li, C.T. Ranjith-Kumar, K. Bhardwaj, A. Holzenburg, P. Li, C.C. Kao, J. Biol. Chem. 283 (2008) 15825–15833.
- [35] D. Bamming, C.M. Horvath, J. Biol. Chem. 284 (2009) 9700-9712.
- [36] C.T. Ranjith-Kumar, A. Murali, W. Dong, D. Srisathiyanarayanan, R. Vaughan, J. Ortiz-Alacantara, K. Bhardwaj, X. Li, P. Li, C.C. Kao, J. Biol. Chem. 284 (2009) 1155–1165.
- [37] K. Malathi, B. Dong, M. Gale Jr., R.H. Silverman, Nature 448 (2007) 816–819.